Electronic Supplementary Material (ESI) for Chemical Science.
This journal is © The Royal Society of Chemistry 2022

Supporting information for

Photosubstitution in a new trisheteroleptic ruthenium complex inhibits conjunctival melanoma growth in zebrafish orthotopic xenograft model

Quanchi Chen [1, 2#], Jordi-Amat Cuello-Garibo [3#], Ludovic Bretin [3], Liyan Zhang [3], Vadde Ramu [3], Yasmin Aydar [2], Yevhen Batsuin [3], Sharon Bronkhorst [3], Yurii Husiev [3], Nataliia Beztsinna [3], Lanpeng Chen [2], Xue-Quan Zhou [3], Claudia Schmidt [4], Ingo Ott [4], Martine J. Jager [5], Albert M. Brouwer [6], B. Ewa Snaar-Jagalska [2*], Sylvestre Bonnet [3*]

[1] Division of Spine Surgery, Department of Orthopedic Surgery, Nanjing Drum Tower Hospital, The Affiliated Hospital of Nanjing University Medical School, Nanjing, China
[2] Institute of Biology, Leiden University, Leiden, The Netherlands
[3] Leiden Institute of Chemistry, Leiden University, P.O. Box 9502, 2300 RA Leiden, The Netherlands
[4] Institute of Medicinal and Pharmaceutical Chemistry, Technische Universität Braunschweig, Beethovenstrasse 55, D-38106 Braunschweig, Germany
[5] Department of Ophthalmology, Leiden University Medical Center, Leiden, The Netherlands
[6] Van 't Hoff Institute for Molecular Sciences, University of Amsterdam, Science Park 904, 1098 XH Amsterdam (The Netherlands)
# These authors contributed equally to the paper
* Correspondence: b.e.snaar-jagalska@biology.leidenuniv.nl ; Tel.: +31-71-527-4980 (E.S.J.); bonnet@chem.leidenuniv.nl ; Tel : +31-71-527-4260 (S.B.);

Table of content

1 Characterization [2]$(PF_6)_2$ 2
2 Photoreactivity 6
3 Photochemical properties of [2]2+ 7
3.1 Quantum yield determination 7
3.2 Singlet oxygen quantum yield 7
3.3 Emission 8
4 ROS generation in cells 9
5 Dose-response curves in conjunctive melanoma, uveal melanoma and prostate cancer cell lines 10
6 [2]$(PF_6)_2$, cisplatin and camptothecin incubation with pUC19 plasmid in the dark condition 11
7 Maximum tolerated dose determination 12

1 Characterization $[2](PF_6)_2$

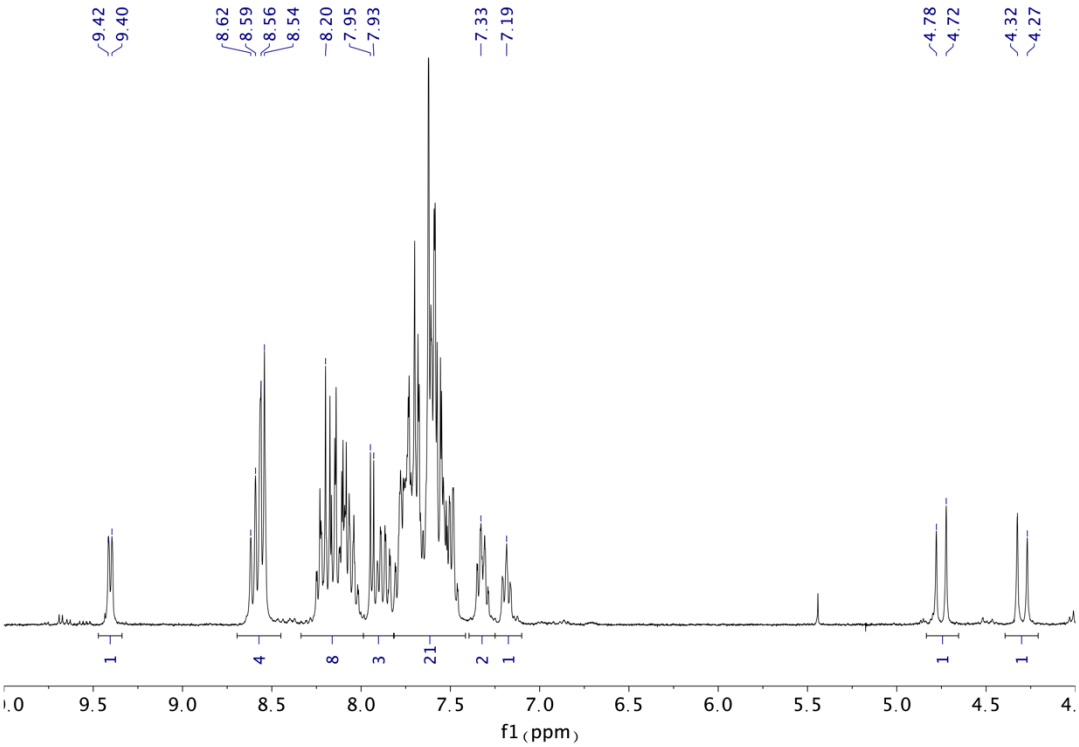

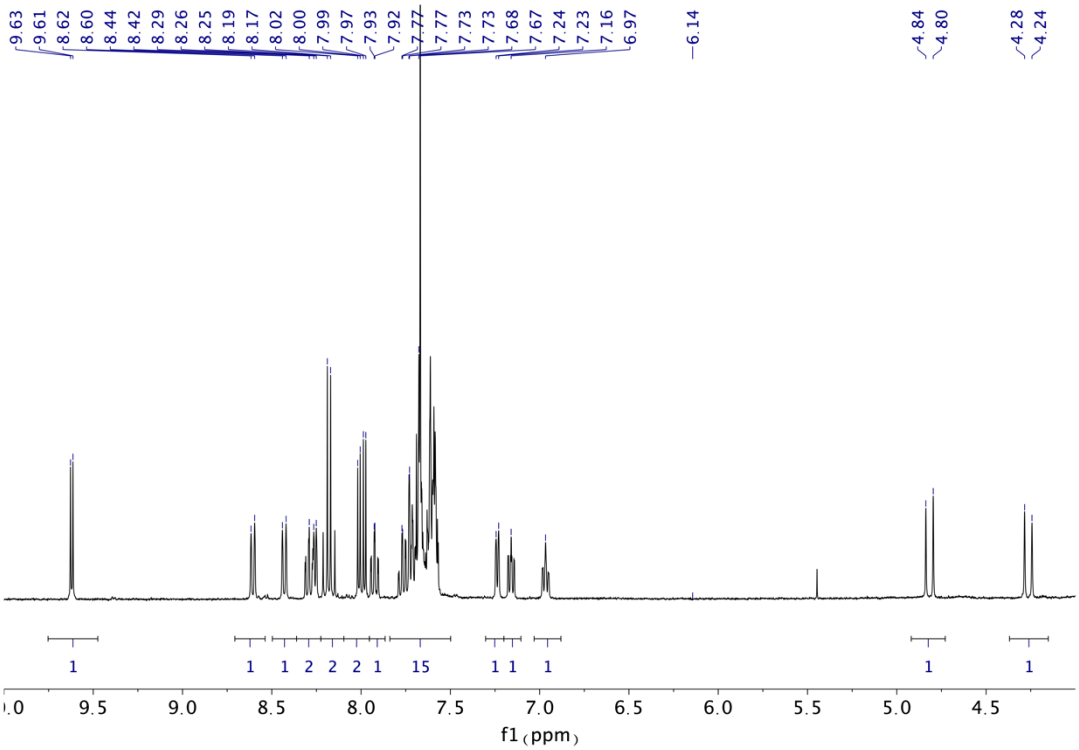

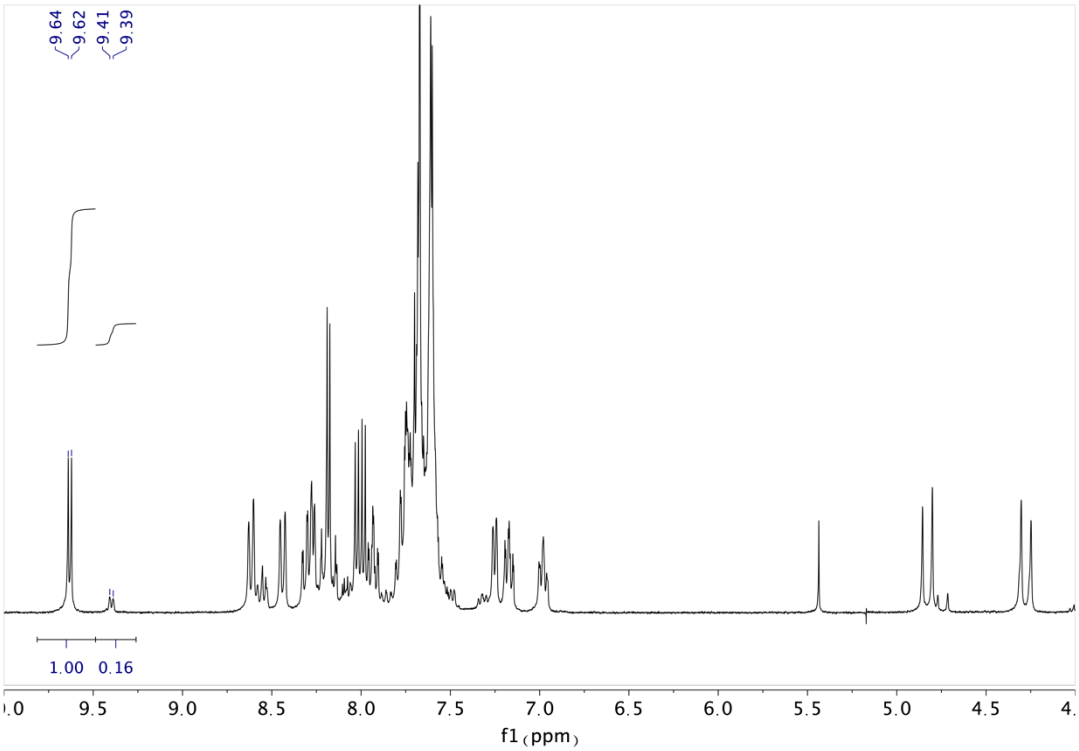

Figure S1. ^{1}H NMR of the two isolated isomers A (top) and B (middle) of [**2**](PF$_6$)$_2$ in CD$_3$CN recorded in the dark using a Bruker DMX-400 spectrometer at 293 K. The bottom ^{1}H NMR spectrum shows a typical mixture of isomers A and B of [**2**](PF$_6$)$_2$, here in a ratio 0.16:1, which were used for photochemical and biological studies.

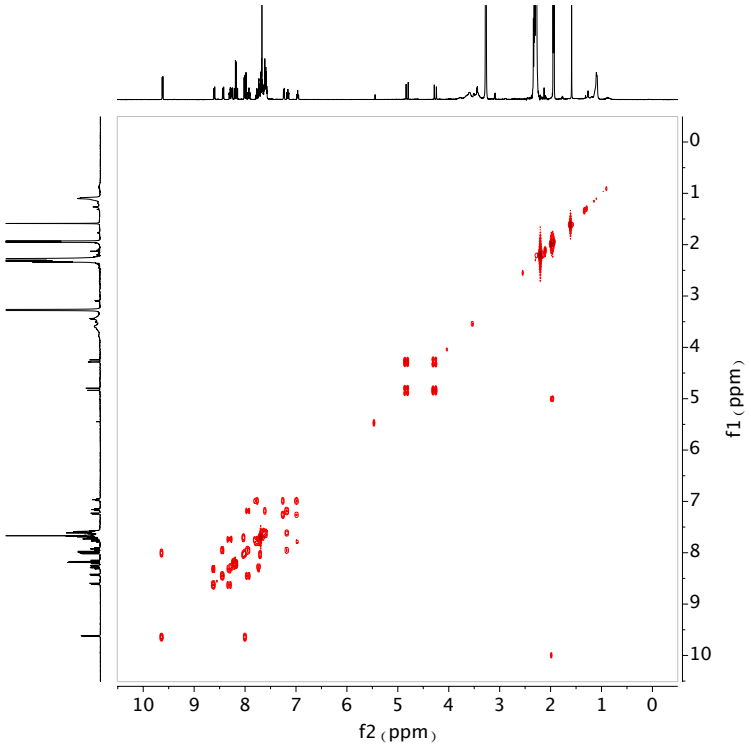

Figure S2. 2D ^{1}H-^{1}H COSY NMR spectrum a solution of isomer B of [**2**](PF$_6$)$_2$ in CD$_3$CN recorded in the dark on a Bruker DMX-400 spectrometer at 293 K.

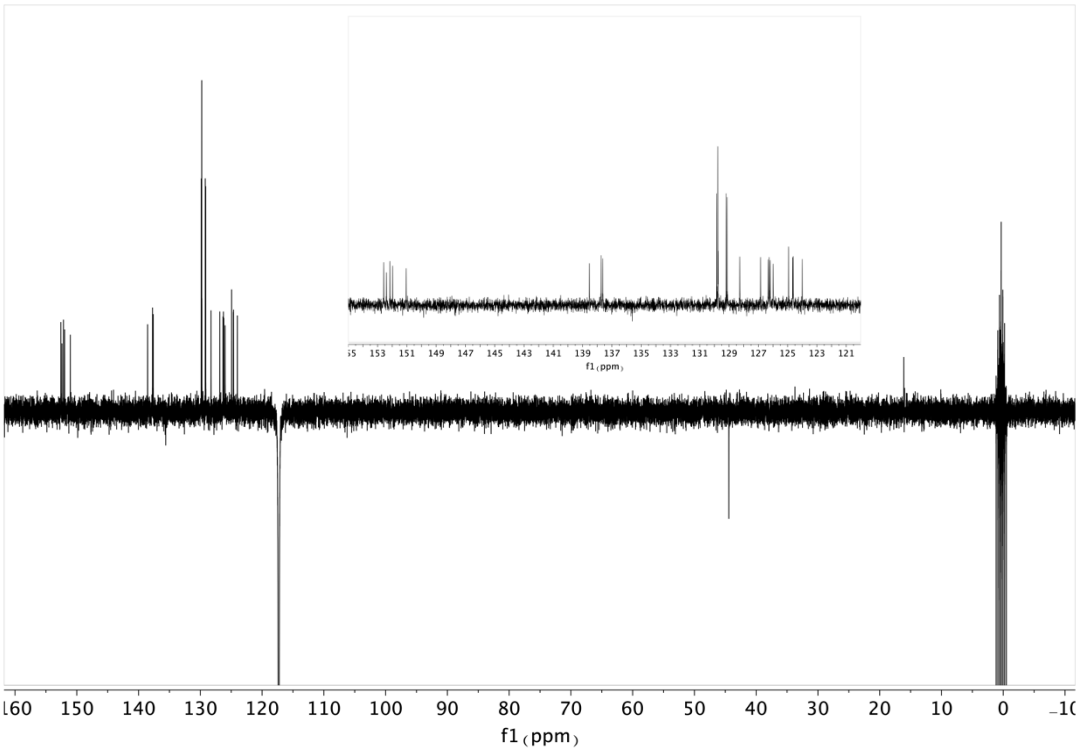

Figure S3. ^{13}C NMR of a solution of isomer B of [**2**]$(PF_6)_2$ in CD_3CN recorded in the dark on a Bruker DMX-400 spectrometer at 293 K.

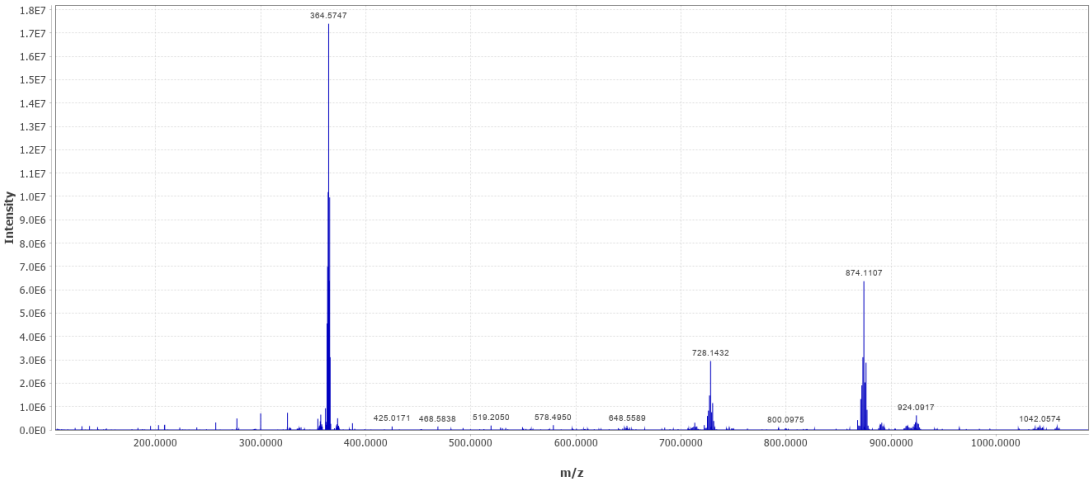

Figure S4. High Resolution Mass Spectrum of [**2**]$(PF_6)_2$ (mixture of isomers A and B, also used in biology) The peaks at 364.5747, 728.1432, and 874.1107, correspond to $[\mathbf{2}]^{2+}$ (calcd 364.5745), [**2**-H]$^+$ 728.1422), and $\{[\mathbf{2}]PF_6\}^+$ (874.1142), respectively.

Mikroanalytisches Laboratorium KOLBE(Nachf.)

Jordi-Amat Cuello-Garibo
Universiteit Leiden
LIC/Metals in Catal, Biomim & Inorg Mat
2333 CC Leiden
The Netherlands

Höhenweg 17
D-45470 Mülheim an der Ruhr

Telefon : +49 - (0)208 - 32502
Telefax : +49 - (0)208 - 382314
www.mikro-lab.de
Date : 20.09.2017

Sample Name	% C	% H	% N	% Dry					Express	V2O5
YB 32	48,21	3,41	6,82	0,79					x	x

Kind regards

Patrick Springer

H. KOLBE Mikroanalytisches Laboratorium D-45470 Mülheim a. d. Ruhr

Figure S5. Elemental Analysis of [**2**]$(PF_6)_2$ (as mixture of A and B isomers) with found values of C, 48.21; H, 3.41; N, 6.82. Calculated values for $C_{41}H_{33}F_{12}N_5P_2RuS$ are C, 48.34; H, 3.26; N, 6.87.

2 Photoreactivity

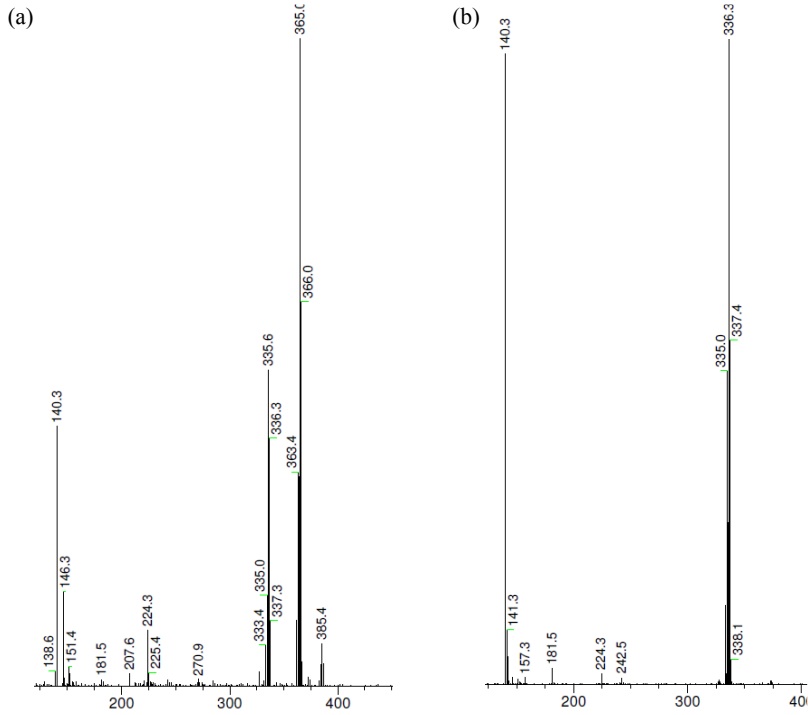

Figure S6. Mass spectrum measured after 2 min (a) and 15 min (b) irradiation with 450 nm light under nitrogen of a 8.86×10^{-4} mol.L^{-1} solution of [**2**]$(PF_6)_2$ in acetonitrile at 25 °C. M/z found (calculated): 365.0 (364.5, [**2**]$^{2+}$), 336.3 (336.08, [Ru(BPhen)(bpy)$(CH_3CN)_2]^{2+}$, 385.4 (385.09, [Ru(BPhen)(bpy)(mtmp)$(CH_3CN)]^{2+}$, 140.3 (140.05) [mtmp + H]$^+$.

3 Photochemical properties of [2]2+

3.1 Quantum yield determination

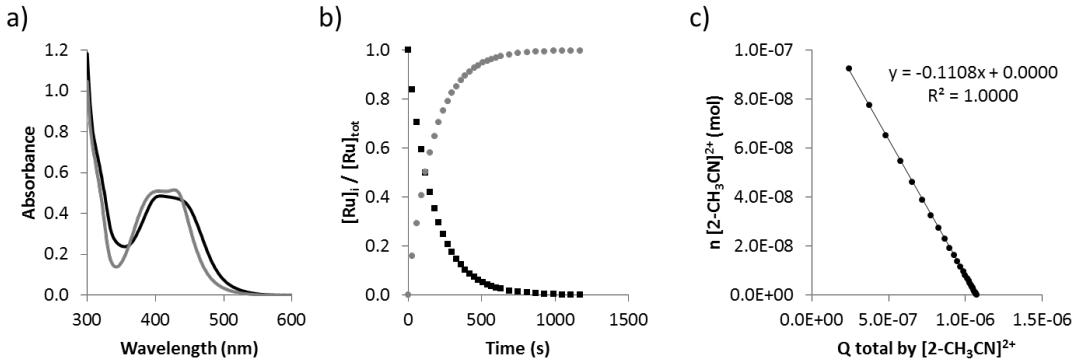

Figure S7. Kinetic data for the second step of the photosubstitution of [**2**](PF$_6$)$_2$ in CH_3CN under N_2. a) Globally fitted absorption spectra of the mono-aqua intermediate [Ru(dpp)(bpy)(η^1-mtmp)(CH_3CN)] ([**2**-CH_3CN] , black) and [Ru(dpp)$_2$(CH_3CN)$_2$]$^{2+}$ (grey) according to modelling using the Glotaran software. b) Modelled evolution of the relative concentrations of [**2**- CH_3CN]$^{2+}$ (squares) and [Ru(dpp)$_2$(CH_3CN)$_2$]$^{2+}$ (circles) vs. irradiation time according to global fitting using Glotaran. c) Plot of the amount of [**2**-CH_3CN]$^{2+}$ (mol) vs. total amount of photons absorbed by [**2**-CH_3CN]$^{2+}$ (mol). The slope of the obtained line is the opposite of the quantum yield of the formation of the bis-aqua complex. Conditions: 0.036 mM solution of [**2**](PF$_6$)$_2$ in CH_3CN irradiated at 298 K under N_2 using a 521 nm LED at $6.21 \cdot 10^{-8}$ mol·s^{-1}.

3.2 Singlet oxygen quantum yield

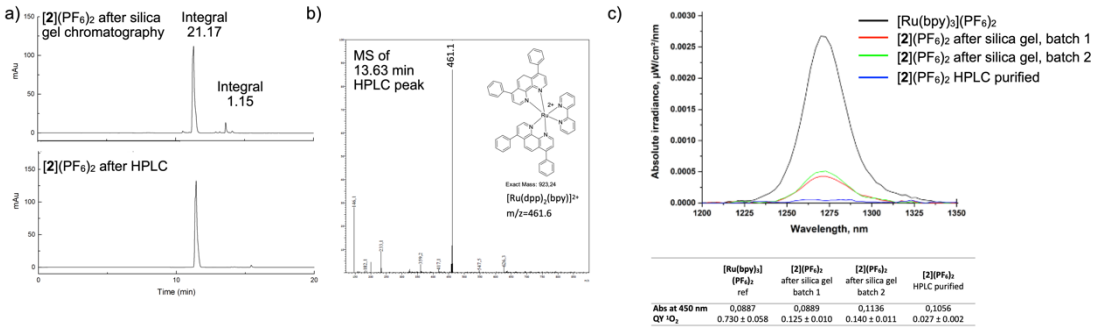

Figure S8. a) HPLC analysis of chromatography-purified and HPLC-purified batches of [**2**](PF$_6$)$_2$. Gradient: 10-90% ACN/H_2O, 20 min, UV channel=280 nm. b) mass spectrum of the t_R=13.63 min impurity, corresponding to the [Ru(dpp)$_2$(bpy)]$^{2+}$ impurity. c) NIR emission from $^1O_2$ generated by different samples of [**2**](PF$_6$)$_2$. Ru(bpy$_3$)Cl$_2$ is used as a reference with reported Φ_Δ ($^1O_2$) = 0.73 ± 8% in air-saturated CD_3OD.[1] Conditions: CD_3OD, 298 K, 50 mW laser power, 450 nm.

3.3 Emission

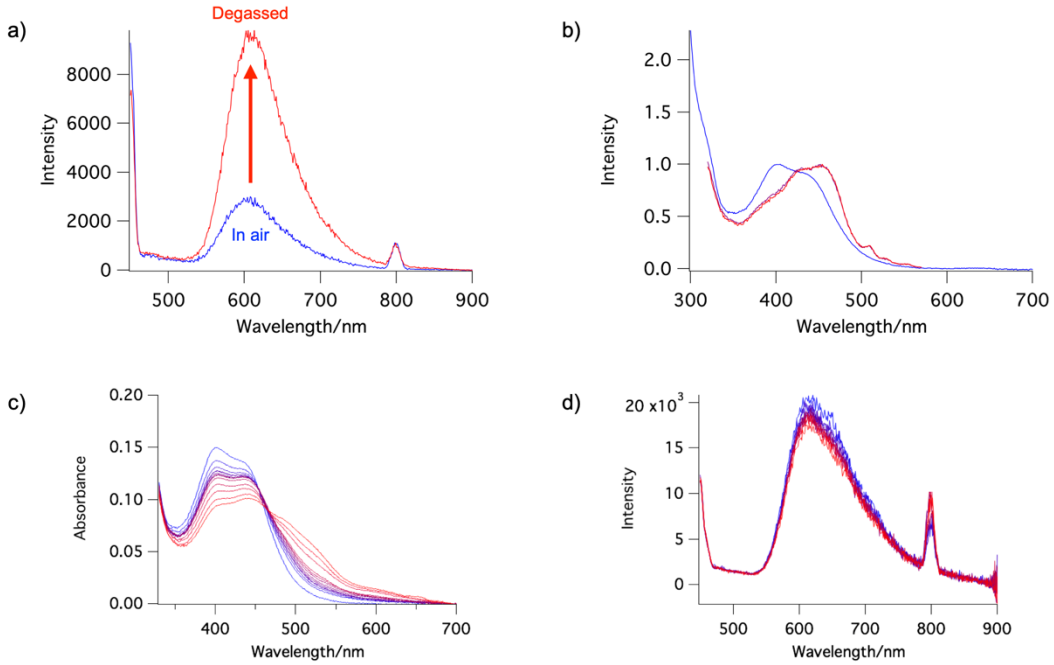

Figure S9. a) Steady-state emission of a sample of [**2**]$(PF_6)_2$ (excited at 400 nm) in aerated MeCN solution and after 30 min degassing with argon, demonstrating the phosphorescence character of the emission. b) Comparison of the excitation spectrum (in duplicate, red) with the absorption spectrum (blue). c) Evolution of the absorption spectrum of the sample while continuously irradiating at 400 nm to perform photosubstitution. d) Evolution of the photoluminescence spectrum under the same conditions. The decrease was relatively small (~15% at a total dose of 2.8 J) even though the absorption has changed considerably. This experiment concludes that the emissive species is different from the photosubstitutionally active species $[\mathbf{2}]^{2+}$.

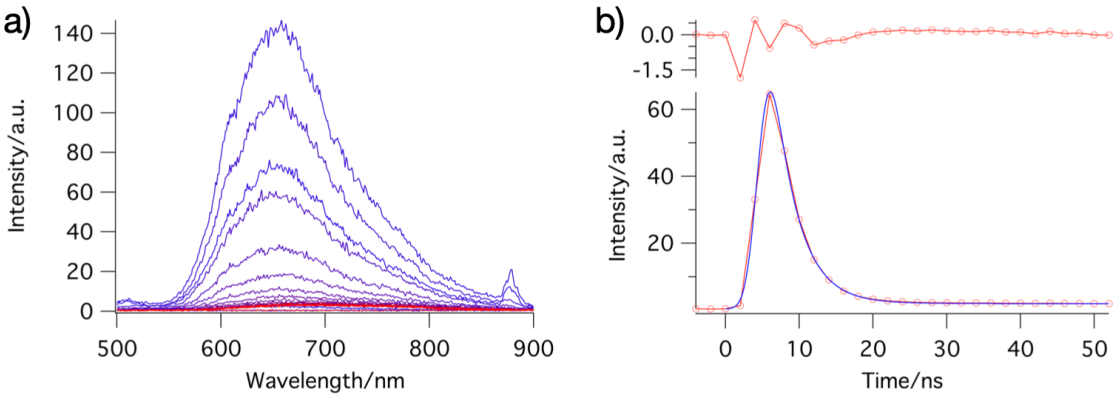

Figure S10. a) Time-resolved emission spectra of a solution of [**2**]$(PF_6)_2$ in argon-saturated MeOH irradiated at 440 nm. Each spectrum integrated over the detector gate width of 2.9 ns, time step 2 ns. b) Spectrally averaged emission intensity vs. time and fitting to a biexpontial decay $I(t) = A_1 e^{-t/\tau_1} + A_2 e^{-t/\tau_2}$ (convolved with a Gaussian instrument response function), and residual (in red). The fast component has a decay time τ_1 =3.2 ns (amplitude A_1=0.986), the long-lived decay due to the impurity was separately measured in a 4 µs time window and fixed here at τ_2 =0.66 µs (amplitude A_2=0.014).

4 ROS generation in cells

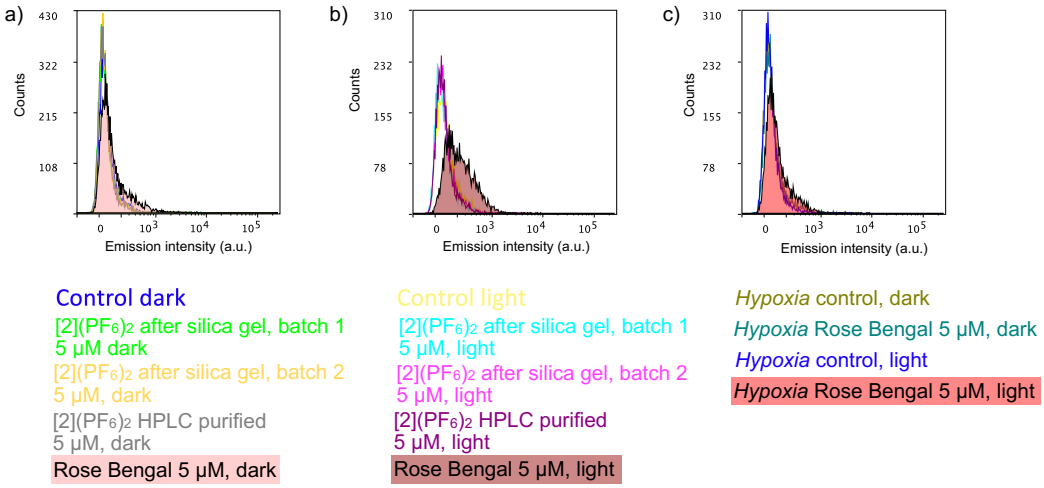

Figure S11. Reactive Oxygen Species generation in CRMM1 cells according to FACS analysis in different conditions using CellROX™ Deep Red Reagent as ROS visualizing agent.

Table S1. Reactive Oxygen Species generation in CRMM1 cells according to FACS analysis using DeepRed dye in different conditions.

	Mean	Median
Control dark	99,46	68,00
[**2**](PF$_6$)$_2$ after silica gel, batch 1, 5 µM, dark	93,23	57,12
[**2**](PF$_6$)$_2$ after silica gel, batch 2, 5 µM, dark	90,19	58,48
[**2**](PF$_6$)$_2$ HPLC purified, 5 µM, dark	82,19	55,76
Rose Bengal, 5 µM, dark	209,33	118,32
Control, **light**	130,14	89,76
[**2**](PF$_6$)$_2$ after silica gel, batch 1, 5 µM, **light**	102,80	68,00
[**2**](PF$_6$)$_2$ after silica gel, batch 2, 5 µM, **light**	110,52	73,44
[**2**](PF$_6$)$_2$ HPLC purified, 5 µM, **light**	110,29	74,80
Rose Bengal, **light**	**299,83**	**216,24**
Hypoxia Control, dark	93,22	59,84
Hypoxia Rose Bengal, dark	111,20	65,28
Hypoxia Control **light**	96,95	54,40
Hypoxia, Rose Bengal, **light**	163,96	99,28

5 Dose-response curves in conjunctive melanoma, uveal melanoma and prostate cancer cell lines

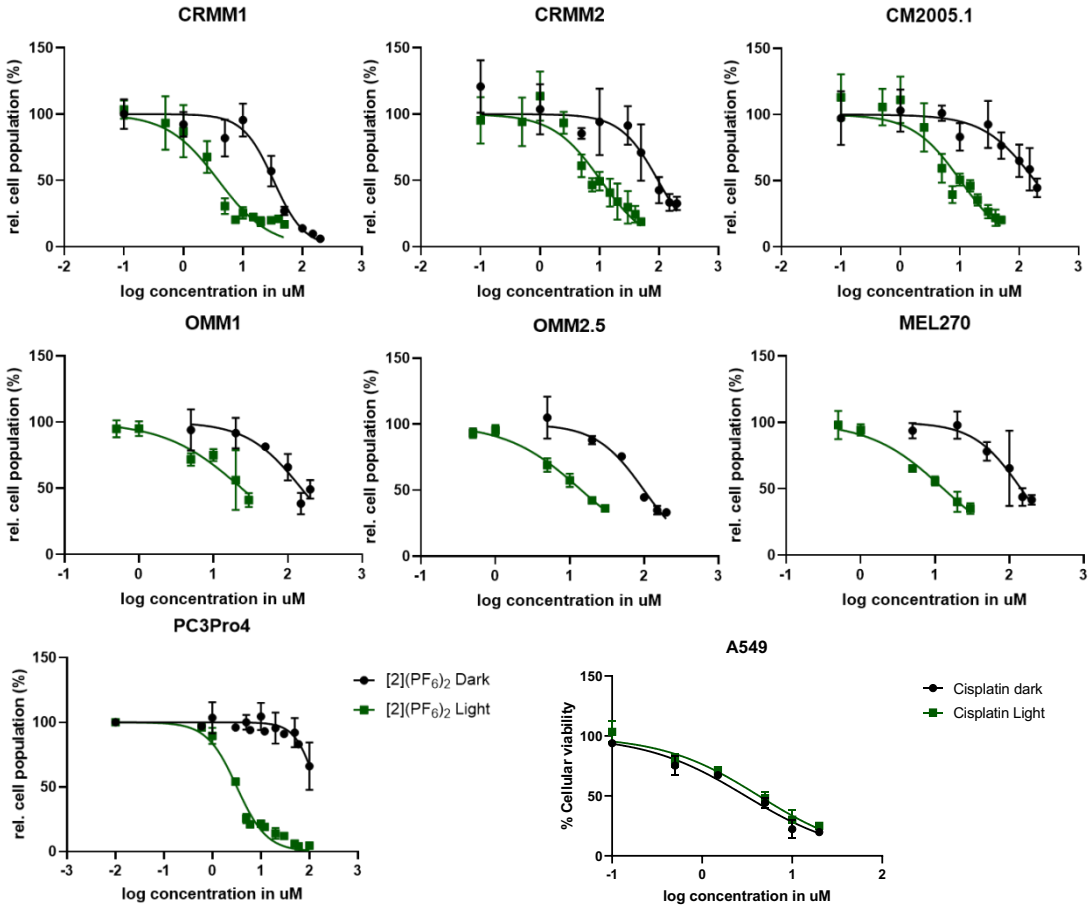

Figure S12. Dose-response curves for CRMM1, CRMM2, CM2005.1, OMM1, OMM2.5, MEL270 and PC3Pro4 cells treated with [**2**]$(PF_6)_2$ and irradiated with green light (520 nm, 21 mW/cm^2, 19 J.cm^{-2}) 24 h after treatment (green data points) or left in the dark (black data points). Control dose-response curves for A549 cells treated with cisplatin in the same conditions. SRB assay was carried out at t=96 h. The absorbance of Sulforhodamine B in solution was measured at 520 nm. Results are presented as means ± SD from three independent experiments.

6 [2](PF$_6$)$_2$, cisplatin and camptothecin incubation with pUC19 plasmid in the dark condition

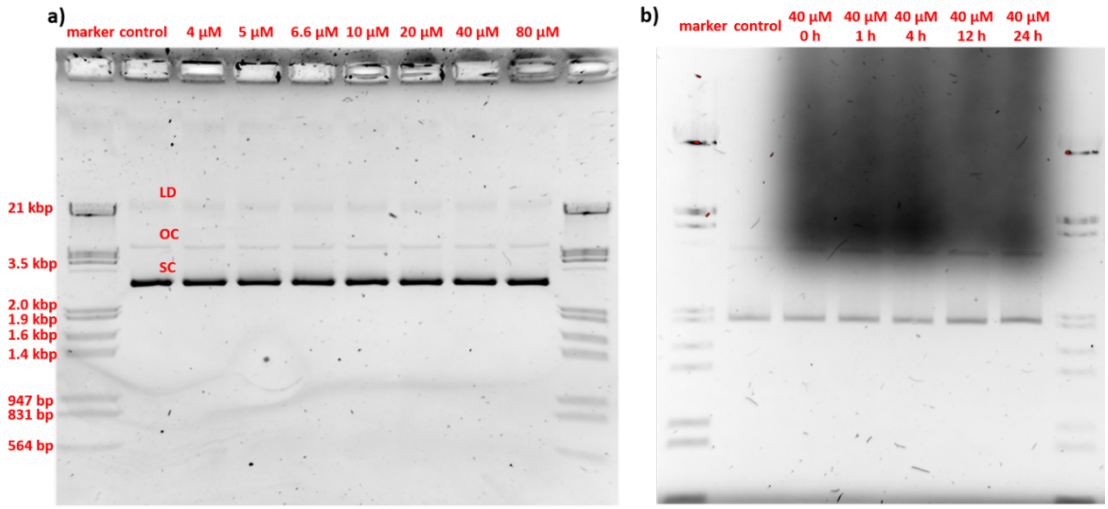

Figure S13. The pUC19 plasmid interacts with [**2**](PF$_6$)$_2$ and camptothecin in the dark. a) Gel electrophoresis for the pUC19 plasmid incubated with different concentrations of [**2**](PF$_6$)$_2$ (4, 5, 6.6, 10, 20, 40, 80 µM) for 24 h in the dark. b) Gel electrophoresis for the pUC19 plasmid incubated with the reference DNA-damaging agent camptothecin (40 µM) for 0, 1, 4, 12 and 24 h in the dark. Condition: incubation at 37 ºC.

	average	stand. dev.
4h Control NIR	1,00	0,00
24h Control NIR	1,00	0,00
4h Control IR	0,82	0,23
24h Control IR	0,86	0,17
4h YB32 IC50 5 µM NIR	0,97	0,08
24h YB32 IC50 5 µM NIR	0,96	0,12
4h YB32 IC50 5 µM IR	1,40	0,11
24h YB32 IC50 5 µM IR	6,22	0,59
4h YB32 IC50+ 10 µM NIR	0,82	0,29
24h YB32 IC50+ 10 µM NIR	0,96	0,14
4h YB32 IC50+ 10 µM IR	4,01	1,20
24h YB32 IC50+ 10 µM IR	11,45	3,38
4h Cisplatin 20 µM	1,05	0,18
24h Cisplatin 20 µM	13,56	1,63
4h Camptothecin 1 µM	2,79	#DIV/0!
24h Camptothecin 1 µM	19,51	#DIV/0!

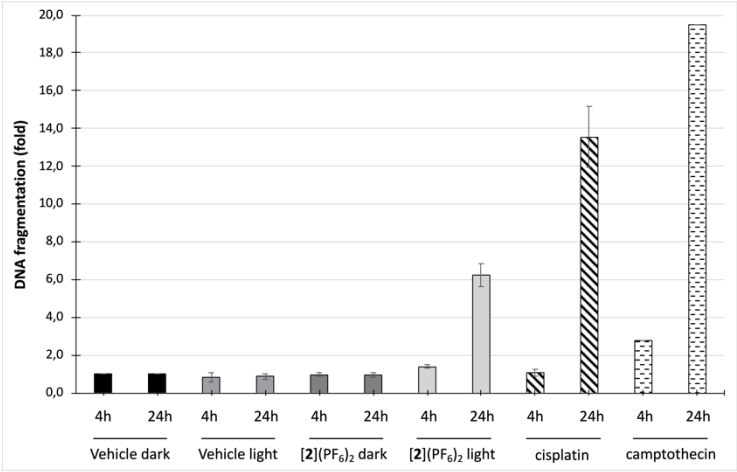

Figure S14. DNA fragmentation in CRMM1 cells treated with [**2**](PF$_6$)$_2$ at EC$_{50,light}$ (4 µM) for 24 h, irradiated or not with green light (520 nm, 15 min, 21 mW.cm^{-2}, 19 J.cm^{-2}), and incubated in the dark for 4 h or 24 h after light irradiation. Control with cisplatin (20 µM) and camptothecin (1 µM) dare also shown. Note: cisplatin and camptothecin doses are not EC$_{50}$ doses but high doses, so it is strictly speaking impossible to compare the DNA fragmentation fold with that of [**2**](PF$_6$)$_2$, which was used at EC$_{50,light}$.

7 Maximum tolerated dose determination

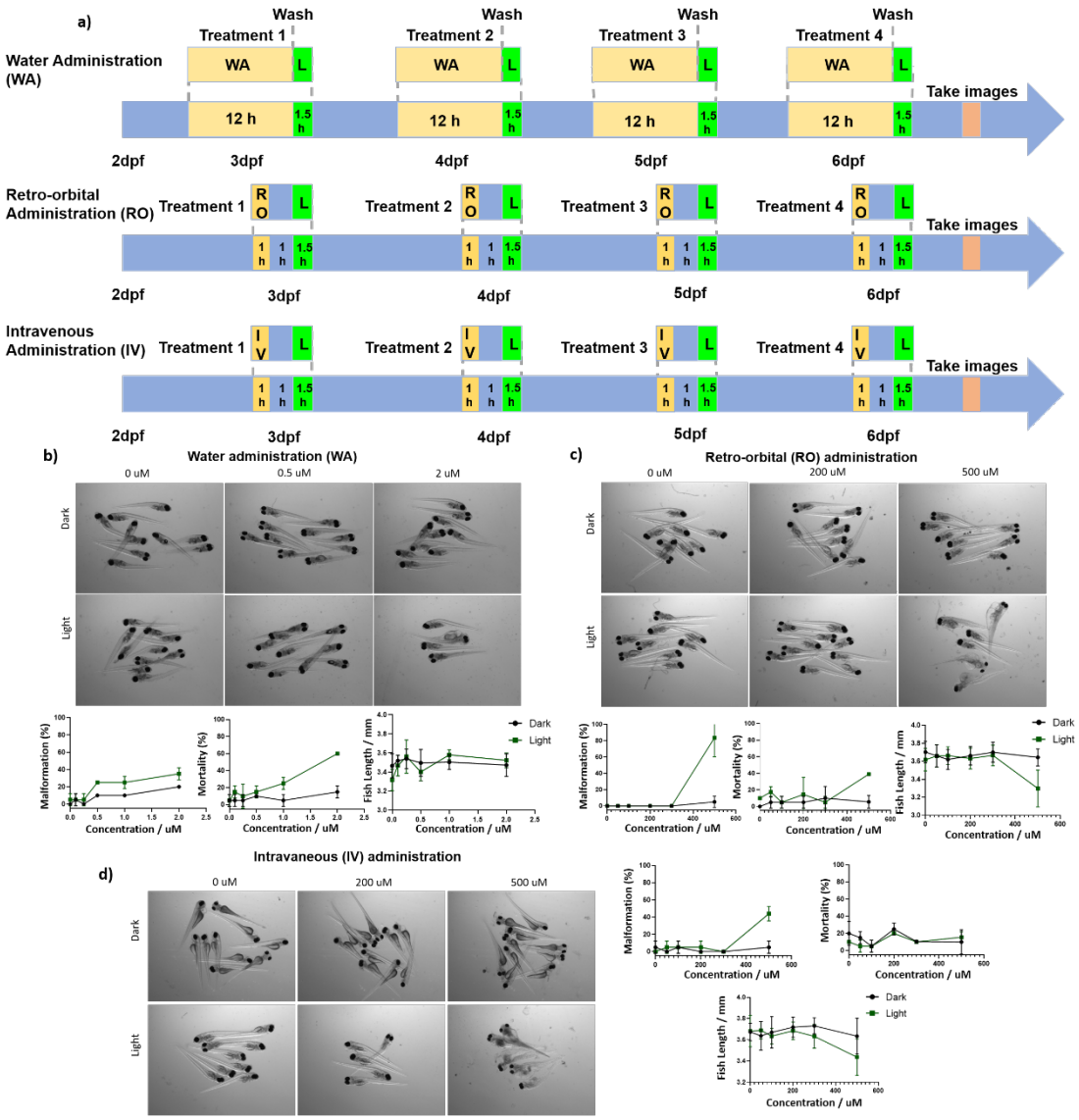

Figure S15. The maximum tolerated dose of [**2**]$(PF_6)_2$ in wild type zebrafish embryos administered through three different routes. **a)** Schedule of [**2**]$(PF_6)_2$ treatment in wild type zebrafish. Water administration (WA): [**2**]$(PF_6)_2$ (0 µM, 0.1 µM, 0.25 µM, 0.5 µM, 1 µM, 2 µM) were added to the water containing 10 embryos per well at 2.5, 3.5, 4.5, 5.5 dpf, for 12h (yellow box). After these treatments, the drug was removed and replaced by egg water followed by 90 min green light irradiation (21 mW/cm^2, 114 J.cm^{-2}, 520 nm), depicted as a green lightning bolt. Intravenous injection (IV) or retro-orbital injection (RO): 1 nL of [**2**]$(PF_6)_2$ (0 µM, 50 µM, 100 µM, 200 µM, 300 µM, 500 µM) were injected into the embryos at 3 dpf to 6 dpf every morning, followed by 60 min drug-to-light interval (yellow box) and 90 min green light irradiation (21 mW/cm^2, 114 J.cm^{-2}, 520 nm), depicted as a green lightning bolt. **b)** WA, c) RO, d) IV. **b-d)** Images were made of irradiated (light) and non-irradiated (dark) embryos (n=30) at 6dpf and the percentages of mortality, malformation and fish length were calculated (shown as means ± SD from three independent experiments). Representative images of embryos under dark and light conditions are shown.

1. D. Garcìa-Fresnadillo, Y. Georgiadou, G. Orellana, A. M. Braun and E. Oliveros, *Helv. Chim. Acta*, 1996, **79**, 1222-1238.